Front. Earth Sci. 2018, 12(3): 468–480
https://doi.org/10.1007/s11707-018-0693-0

RESEARCH ARTICLE

Drift analysis of MH370 debris in the southern Indian Ocean

Jia GAO[1,2,3], Lin MU (✉)[1,3], Xianwen BAO[1], Jun SONG[4], Yang DING[1]

1 College of Oceanic and Atmospheric Sciences, Ocean University of China, Qingdao 266100, China
2 National Marine Data and Information Service, Tianjin 300171, China
3 College of Marine Science and Technology, China University of Geosciences, Wuhan 430074, China
4 School of Marine Science and Environment Engineering, Dalian Ocean University, Dalian 116023, China

Abstract Malaysian Airlines Flight MH370 disappeared on 8 March 2014, while flying from Kuala Lumpur to Beijing. A flaperon from the flight was found on Reunion Island in July 2015. Two more confirmed pieces of debris were found in Mauritius and Tanzania, and 19 unconfirmed items were found off Mozambique, South Africa, and Madagascar. Drift buoys originating from the designated underwater search area arrived in Reunion Island, Mauritius, and Tanzania. Some of these buoys took a similarly long time as did real debris to reach these destinations, following a heading northeast and then west. For the present study, a maritime object drift prediction model was developed. "High resolution surface currents, Stokes drift, and winds" were processed, and a series of model experiments were constructed. The predicted trajectories of the modeled objects were similar to the observed trajectories of the drift buoys. Many modeled objects drifted northward then westward, ending up in Reunion Island, Mauritius, and Tanzania with probabilities of 5‰, 5‰, and 19‰, respectively. At the end of the simulation, most objects were located near 10°S in the western Indian Ocean. There were significant differences between experiments with different leeway factors, possibly because of the influence of southeast trade winds. The north part of the underwater search area is most likely to be the crash site, because the predicted trajectories of objects originating here are consistent with the many pieces of debris found along the east coast of Africa and the absence of such findings on the west coast of Australia.

Keywords MH370, debris, drift trajectory, drift buoys, surface currents, Stokes drift

1 Introduction

On 8 March 2014, a Boeing 777-200ER aircraft operating as Malaysia Airlines Flight MH370 on a scheduled passenger service from Kuala Lumpur, Malaysia to Beijing, China disappeared from air traffic control radar with 227 passengers and 12 crew members on board. A multinational search effort began in the Gulf of Thailand and the South China Sea, and was soon extended to the Strait of Malacca and the Andaman Sea. Analysis of satellite communications between the aircraft and Inmarsat's satellite concluded that the flight flew south into the southern Indian Ocean (Ashton et al., 2015), although the precise location could not be determined. Australia took charge of the search effort on 17 March, when the search shifted to the southern Indian Ocean. On 24 March 2014, the Malaysian government noted that the final known location of MH370, as determined by satellite communication, was far from any possible landing sites, and concluded that the flight had ended in the southern Indian Ocean. Despite the largest and most expensive search in aviation history, nothing was found of the aircraft until 29 July 2015, when a piece of marine debris, later confirmed to be a flaperon from MH370, was found on Reunion Island, about 17 months after the flight went missing. Two more pieces of debris confirmed to be from the aircraft were found on the Island of Rodrigues, Mauritius and Pemba Island, Tanzania in May and June 2016; a further 19 items almost certainly from MH370 or under evaluation were found off Mozambique, South Africa, and Madagascar[1)]. Despite many more pieces of debris being found in 2016, the search for MH370 was suspended on 17 January 2017.

The pieces of debris were carried from the crash site to the areas where they were ultimately found in the western Indian Ocean by the general cyclonic ocean circulation in the southern Indian Ocean. Several operational systems

Received June 27, 2017; accepted November 23, 2017

E-mail: moulin1977@hotmail.com

1) Malaysian ICAO Annex 13 Safety Investigation for MH370 (2016). Summary of possible MH370 debris recovered (Updated 14 October 2016).

have been developed for use in marine search and rescue. Canadian Maritime Search and Rescue Planning (CANSARP) is a complex tool that has been used extensively in Canadian rescue centers since the early 1990s[1)]. Leeway, the operational search and rescue model for the Norwegian Sea and the North Sea, rapidly returns search areas based on prognoses of wind and surface currents (Breivik and Allen, 2008). Few studies on drift analysis of MH370 debris have been published. Eichhorn and Haertel (2016) used a backwards flow simulation method to simulate the possible location of the debris without considering wind and waves. Jansen et al. (2016) simulated the movement of floating debris using currents and winds; the results showed that the west coast of Africa and the southeast coast of Australia were likely places for debris to be found. Gao et al. (2016) estimated the trajectory of debris using surface currents with 1/3° and 5-day interval resolution.

The area considered to have highest probability of being the crash area is a 700-km-long belt, as shown in Fig. 1, known as the underwater search area (UWSA) or 7th arc (ATSB, 2015, 2016). For ease of numerical simulation, this research defines the possible air crash area as the square region with four vertices (91.8°E, 35°S), (92.8°E, 36.1°S), (86.2°E, 40°S), and (85.2°E, 38.9°S). The Reunion Island, Mauritius, and Tanzania areas are defined as the circular regions within a radius of 100 km of (57°E, 21.2°S), (63.4°E, 19.7°S), and (39.8°E, 5.2°S), respectively.

In the present study, aircraft debris is assumed to drift on the surface and to be affected by wind. Vertical movement is assumed to be negligible. The wave effect should be considered as Stokes drift makes a significant contribution to surface currents (Polton et al., 2005), especially in the Southern Ocean (Hui and Xu, 2016), it is between 0.6% and 1.3% and of similar magnitude as the direct wind-induced current (that is 1%–1.8% of wind speed) (Ardhuin et al., 2009). Therefore, the present study uses high-resolution ocean surface currents, Stokes drift, and winds to simulate the drifting pathways of debris from the underwater search area along the 7th arc.

The rest of this paper is organized as follows: Section 2 describes the data sets used. Section 3 describes the method we used to calculate objects drifting under the influence of currents, winds and waves (Stokes drift). Section 4 gives results and analysis. Finally, the summary and conclusions are presented in section 5.

2 Data and processing

2.1 Drift data

The drift data were collected from satellite-tracked surface drift buoys from the Global Drifter Program (GDP), which is part of the Global Ocean Observing System. The GDP program originated in 1979 and a large number of drifters have been deployed in the ocean. Each drifter consists of a surface buoy and a subsurface drogue (sea anchor), attached by a long thin tether. The drogue is centered at about 15 m beneath the sea surface. The 0–15-m layer sea water is assumed to be the surface layer, as the current of this layer is similar in the deep ocean. The mean depth of the Indian Ocean is 3893 m; as a result, the trajectories of the debris can be estimated by the drifters as they are assumed to drift in the surface layer.

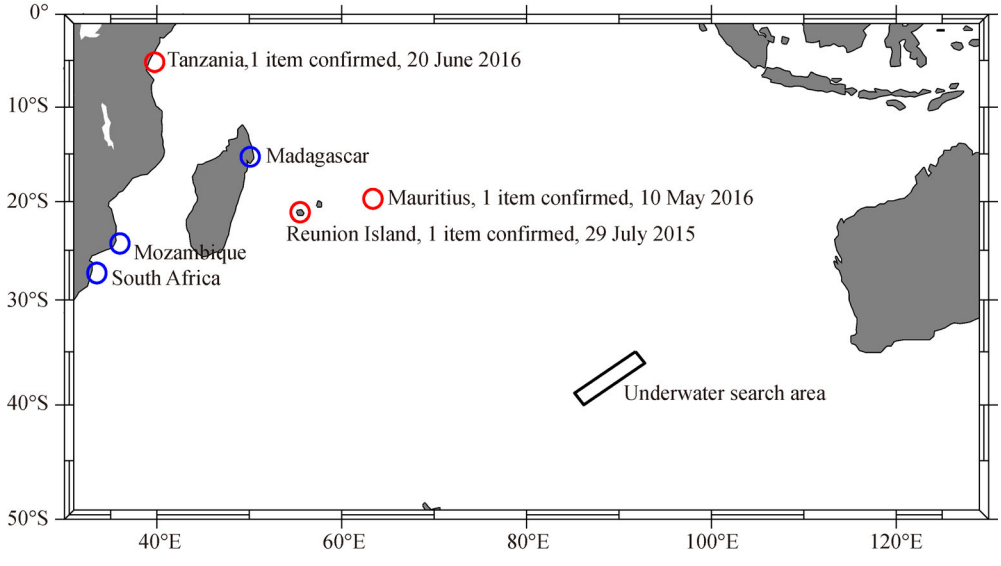

Fig. 1 Underwater search area (UWSA) and areas where possible debris recovered. The black box is the UWSA; red circles indicate where confirmed debris was found; blue circles indicate where unconfirmed items were found.

1) Fisheries and Oceans Canada Canadian Coast Guard (200 9). CANSARP User Manual.

2.2 Ocean surface current data

Surface current data was extracted from the global Hybrid Coordinate Ocean Model (HYCOM) with 1/12° resolution reanalysis outputs at daily intervals. The system uses the Navy Coupled Ocean Data Assimilation (NCODA) system for data assimilation (Fox et al., 2002; Cummings, 2005; Cummings and Smedstad, 2013). The HYCOM reanalysis data has been validated and widely used (Chassignet et al., 2009; Joseph et al., 2012; Yin et al., 2017). The surface current data used in the present study are the sum of the HYCOM surface currents and the Stokes drift computed from the European Center for Medium-Range Weather Forecasts (ECMWF) interim sea surface wave data. The ECMWF data contain three variables that are used to calculate the Stokes drift: mean wave direction, mean wave period, and significant wave height. The ERA interim data have been validated and widely used for meteorological and oceanic studies (Dee et al., 2011; Campos and Soares, 2016). The ERA interim wave data are extracted with a 6-hour time average and a spatial resolution of 1/4°. The Stokes drift velocity at the sea surface U_S is given by Philipps (1977):

$$\boldsymbol{U}_S = U_S \mathrm{e}^{2kz} \hat{\boldsymbol{k}},\ U_S = a^2 \sigma k, \tag{1}$$

in which U_S is the Stokes drift velocity at the sea surface, and $\hat{\boldsymbol{k}}$ is the unit wavenumber vector. On the basis of the deep water dispersion relation, $\sigma = \sqrt{gk} = \dfrac{2\pi}{T}$, we get:

$$k = \frac{4\pi^2}{gT^2}, \tag{2}$$

in which T represents the mean wave period provided by ECMWF data. Combined with Eq. (1), using the modeled significant wave height $H_S\left(a = \dfrac{1}{2}H_S\right)$ and mean wave direction θ from ECMWF, we derive the following:

$$\boldsymbol{U}_S = \frac{2\pi^3 H_S^2}{gT^3} \cdot \mathrm{e}^{\frac{8\pi^2}{gT^2}z} \cdot (\sin\theta + i \cdot \cos\theta),\ U_S = \frac{2\pi^3 H_S^2}{gT^3}. \tag{3}$$

Figure 2 shows that the annual mean Stokes drift velocity is greater than 0.1 m/s in mid-to-high latitudes and its direction is consistent with the strong prevailing west wind. In mid-to-low latitudes it corresponds to the southeast trade wind. A cyclonic gyre exists, and the velocity is higher in eastern areas than in western areas because it is located in the Southern Hemisphere.

2.3 Wind data

The Climate Forecast System Reanalysis (CFSR) was designed as a global high-resolution coupled atmosphere–ocean–land surface–sea ice system to provide the best estimate of the state of these coupled domains over the 32-year period from January 1979 to March 2011. It has since been extended as an operational real-time product (Saha et al., 2014). The CFSR wind data with spatial and temporal resolution of 0.313°× 0.312° and 6 hours, respectively, were processed to 0.1°× 0.1° and 1 hour, respectively, using optimal interpolation. The CFSR reanalysis has been validated and extensively used to characterize near-surface wind variability (Rimac et al., 2013; Rahn and Garreaud, 2014; Mo et al., 2016; Yu et al., 2016; Montecinos et al., 2017). The NCEP and ERA datasets have been compared by many researchers. The reanalysis solutions are driven by similar model dynamics and largely assimilate common datasets, so they show good consistency (Alves and Robert, 2005; Chaudhuri et al., 2013).

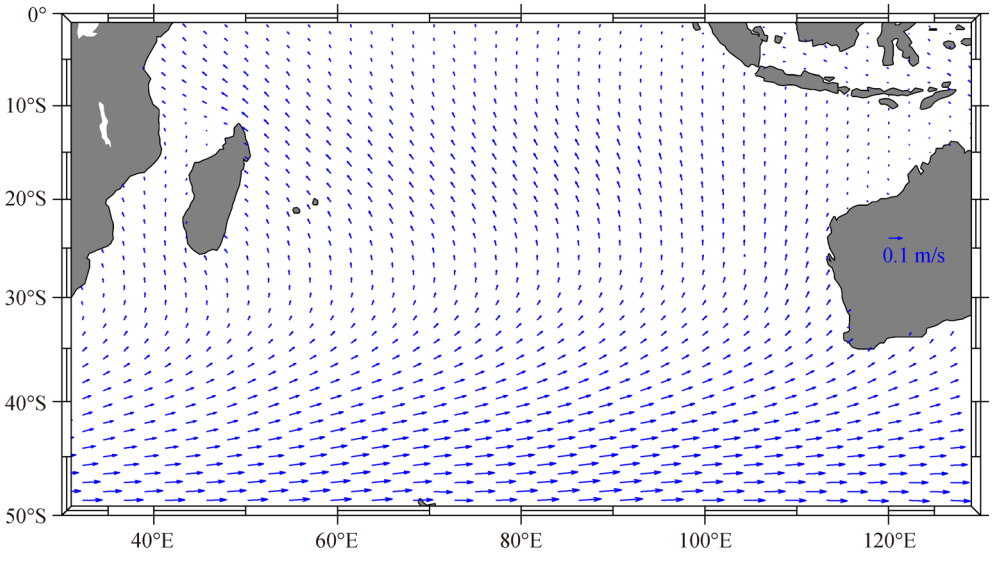

Fig. 2 Annual mean Stokes drift in the southern Indian Ocean in 2014.

3 Methods

Because the number of samples is insufficient to provide statistically significant results, a maritime objects drift prediction model based on the Leeway model is used to produce a great number of simulated drift trajectories of objects deployed in possible air crash sites along the 7th arc.

3.1 Maritime objects drift prediction model

The motion of a drifting object on the sea surface is the net result of the wind, current and wave forces acting on it. The leeway of a drifting object is defined as its motion due to wind and waves relative to the ambient current. It is decomposed into downwind leeway (DWL) and crosswind leeway (CWL) (Breivik and Allen, 2008). Field studies have been carried out to determine how different classes of objects respond to the wind (Allen, 2005). Objects have various magnitudes of DWL and CWL depending on the shape and buoyancy characteristics of the object. In the present study, the CWL is ignored because the coefficients of aircraft debris are unknown and there is a lack of direct field data. The drifting velocity of a sea surface object is obtained from:

$$V_{\text{object}} = V_{\text{current}} + \alpha V_{\text{wind}}, \tag{4}$$

in which V_{object} is the velocity of a drifting object near the sea surface, V_{current} is the velocity of the surface current (defined as the sum of HYCOM surface currents and Stokes drift), V_{wind} is the velocity of the wind (reference height 10 m), and α is wind drift coefficient (DWL factor).

The position of a drifting object is the sum of current-induced drift and wind-induce drift, obtained from:

$$\begin{aligned} x(t) - x_0 &= \int_0^t V_{\text{object}}(t')\mathrm{d}t' \\ &= \int_0^t [V_{\text{current}}(t') + \alpha V_{\text{wind}}(t')]\mathrm{d}t, \end{aligned} \tag{5}$$

where $x(t)$ is the position of drifting object at time t, x_0 is the origin position.

The drifting object is defined as a Lagrangian particle drifting independently. The Monte Carlo method is adopted, and a great number of particles are dispersed in UWSA. Taking wave-induced Stokes drift into account, a particle dispersion model is applied in the southern Indian Ocean. A second-order Runge–Kutta scheme is used for the computation of Lagrangian advection of individual particles on a sphere.

3.2 Design of numerical experiments

To increase the sample size, we simulated a great number of particle trajectories. In searching for drifting objects on the sea surface, a large number of unknowns must be quantified and the most probable search area must be estimated. In addition to perturbing the leeway coefficients and the forcing fields, an operational model must vary the initial position and release time of the object to account for the uncertainty in the last known position (Breivik and Allen, 2008). The first task in a search is to determine the initial position and release time of the object. As shown in Table 1, three cases were designed to compare different trajectories with 5-day intervals in March 2014. Case 1 started at 0:00 on 3 March, Case 2 started on 8 March, and Case 3 started on 13 March 2014. A typical wind drift coefficient of 1.5% is given because of the lack of direct field studies on aircraft flaperons. Two other coefficients of 1.2% and 1.8% are also considered, to account for the diversity of the items found, for a total of nine experiments – three for each of the start time cases. 1116 objects with 0.1° distance to each other were released in UWSA in each experiment. The model computation domain is 30°–130°E and 50°–0°S, and the integration time step is 1 hour. Experiments are repeated with and without Stokes drift to compare the influence of Stokes drift on drifting objects. In total, 18 experiments with 20,088 trajectories of drifting particles were obtained.

Table 1 Design of experiments with and without Stokes drift

Serial number		Start date	Leeway factor
Case 1	Exp. 1	3 March, 2014	1.2%
	Exp. 2	3 March, 2014	1.5%
	Exp. 3	3 March, 2014	1.8%
Case 2	Exp. 4	8 March, 2014	1.2%
	Exp. 5	8 March, 2014	1.5%
	Exp. 6	8 March, 2014	1.8%
Case 3	Exp. 7	13 March, 2014	1.2%
	Exp. 8	13 March, 2014	1.5%
	Exp. 9	13 March, 2014	1.8%

4 Results

4.1 Surface drift buoys

We extracted from the 1979−2015 database the trajectories of all drifters relevant to MH370, i.e. drifters that were near the defined possible crash area along the 7th arc. 94 drifters passed through the UWSA, and 61 of them reported data for more than 1 year after that. Among these, a small number of them moved to east and north, while most of them moved to northeast and then turn northwest or southwest, the former drifters can reach east coast of Africa through waters north of Madagascar, while the latter drifters reach the east coast of Africa through waters south of Madagascar (Fig. 3).

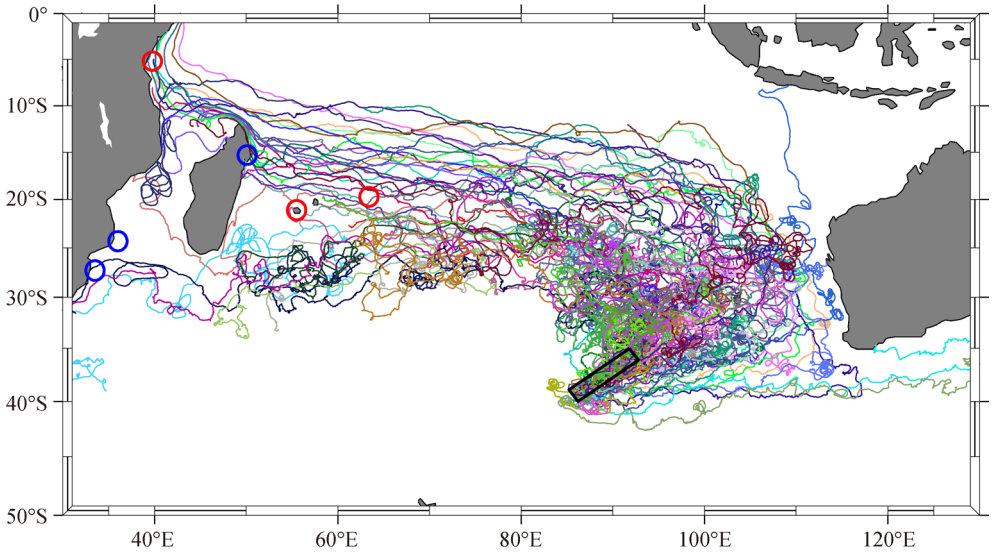

Fig. 3 Trajectories of surface drifting buoys originate from the UWSA and last more than 1 yr. The black box is the UWSA; red circles indicate where confirmed debris was found; blue circles indicate where unconfirmed items were found.

Then the trajectories of these drifters were examined one by one to identify pathways and time to enter the Reunion Island area, the Mauritius area, and the Tanzania area. The statistical results are shown in Table 2, Table 3, and Table 4. Three buoys drifted northeast and then west to arrive in the Reunion Island area (Fig. 4(a)), taking 593–732 days; one of these buoys originated from 11 March, close to the time that MH370 was lost. Five buoys drifted north or northeast and then west, arriving in the Mauritius area (Fig. 4(b)) after 400–1552 days; one buoy originated from 20 March. Six more buoys drifted east or north, then turned west when they were affected by the South Equatorial Current between 10°S and 20°S. These buoys passed north of Madagascar and reached Pemba Island, Tanzania (Fig. 4(c)), taking 481–1013 days; one of the buoys originated from 20 March. Neither inter-annual nor seasonal tendency was found according to the origin dates of the buoys originating in the UWSA. It represents a certain universality and possibility that buoys can drift to the areas where debris were found under the influence of comparatively stable ocean circulation and winds in southern Indian Ocean.

Analysis of surface buoy data indicates that buoys originating from the UWSA can drift to areas where confirmed debris were found, such as Reunion Island, Mauritius and Tanzania, in a similar timeframe to that of actual drifting debris. Some buoys can also drift to the areas where items were found but not confirmed to be from the aircraft, such as Madagascar, Mozambique and South Africa. The estimated results of drifting trajectories and time scales from surface drifting buoys give us a good reference in terms of annual mean currents and winds, though the found buoys passed the UWSA not only in March but also in other months.

Table 2 Information of buoys arriving in the Reunion Island area

Buoy ID	Origin time in possible air crash area	End time in Mauritius area	Duration/ days
34160	20030310	20041104	604
46048	20071109	20090625	593
70854	20071031	20091102	732

Table 3 Information of buoys arriving in the Mauritius area

Buoy ID	Origin time in possible air crash area	End time in Mauritius area	Duration/ days
2339263	20050320	20060425	400
46044	20060925	20080519	601
62576	20110213	20120414	425
9525791	19970524	20010823	1552
9525837	19980803	20020810	1467

Table 4 Information of buoys arriving in the Tanzania area

Buoy ID	Origin time in possible air crash area	End time in Tanzania area	Duration/ days
2339263	20050320	20060714	481
30723	20030422	20040916	512
44055	20060731	20080405	613
46036	20051115	20080824	1013
53417	20070704	20081031	485
63814	20080101	20090609	524

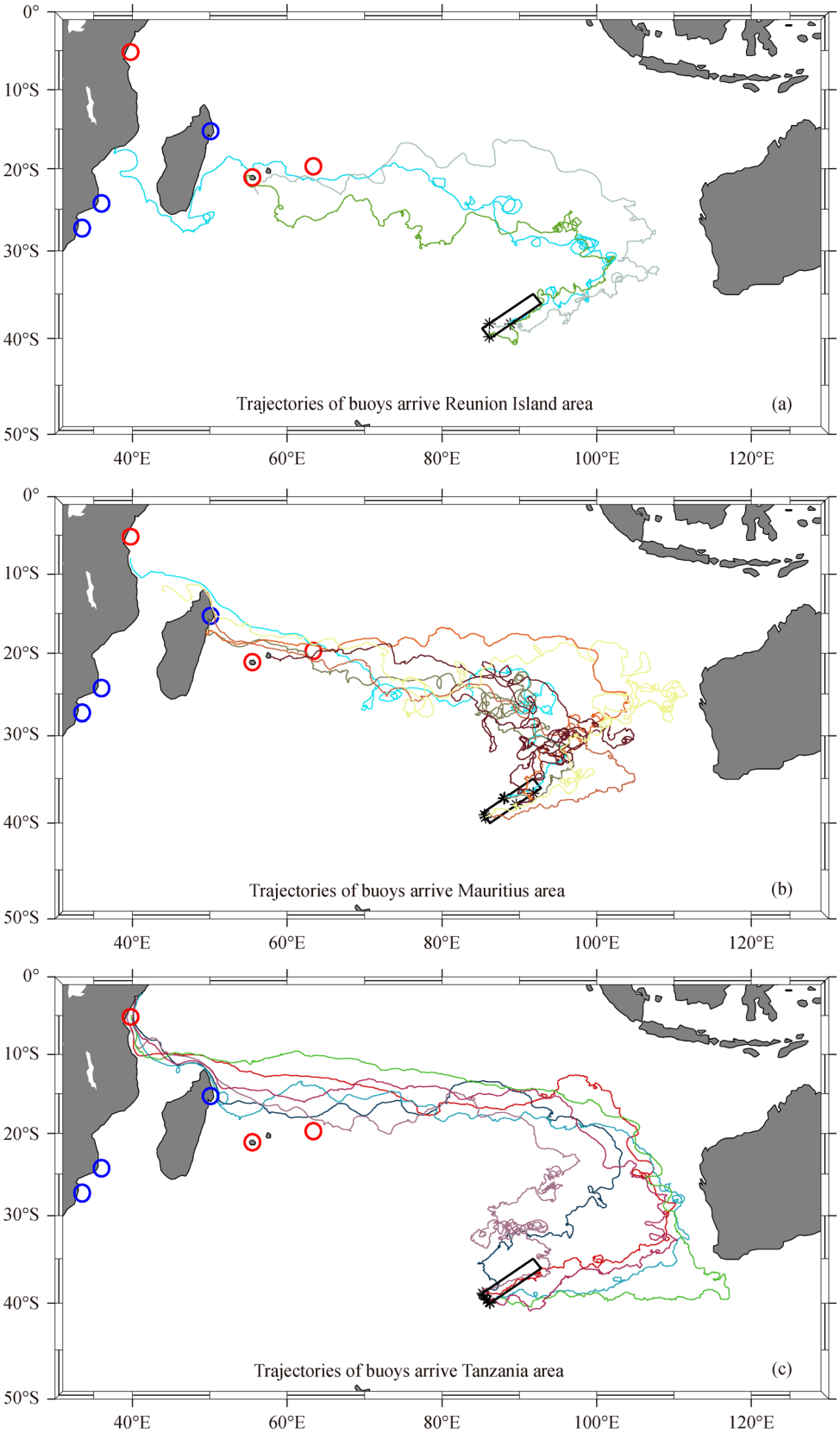

Fig. 4 Trajectories of surface drifting buoys originating from the UWSA and enter the Reunion Island area, the Mauritius area, and the Tanzania area. The black box is the UWSA; red circles indicate where confirmed debris was found; blue circles indicate where unconfirmed items were found.

4.2 Simulation results

The results of the three cases are basically of the same frame. Owing to the limitation of space, some trajectories in Experiment 5 (start time is 8 March and leeway factor is the typical value of 1.5%) are given in Fig. 5 as an example. Two additional experiments are added into Experiment 5, 61 objects are released at the same position with the 61 surface drift buoys which were found in Section 4.1. The trajectories of objects with (Fig. 5(b)) and without Stokes drift (Fig. 5(a)) are provided for comparison. The trajectories with Stokes drift (Fig. 5(b)) are more consistent with the surface drift buoys (Fig. 3), supporting the effectiveness of including Stokes drift in the simulation. The majority of objects move to northeast from the area along the 7th arc under the influence of the cyclone circulation system in the southern Indian Ocean. They then turn west when arriving in mid–low latitudes under the effect of the South Equatorial Current. Some objects reach Mauritius or Reunion Island, some pass through waters north or south of Madagascar and then reach Tanzania or Mozambique. Without Stokes drift, many more objects drift eastwards. The visible difference between the trajectories of objects and buoys is mainly due to different day and time of origin. The unknown time and location of the air crash leads to much uncertainty in the simulation.

Figure 6 and Figure 7 show the predicted final locations of objects at midnight on 30 July 2015, after drifting for 500 days. The final locations of the three simulation cases that started at five-day intervals are not significantly different from each other. In experiments with Stokes drift, a great number of objects passed around 10°S in the south Indian Ocean, where the South Equatorial Current flows from east to west. Many of these objects ended up along the east coast of Africa or near Madagascar. Other objects ended up on the southwest coast of Australia or the south

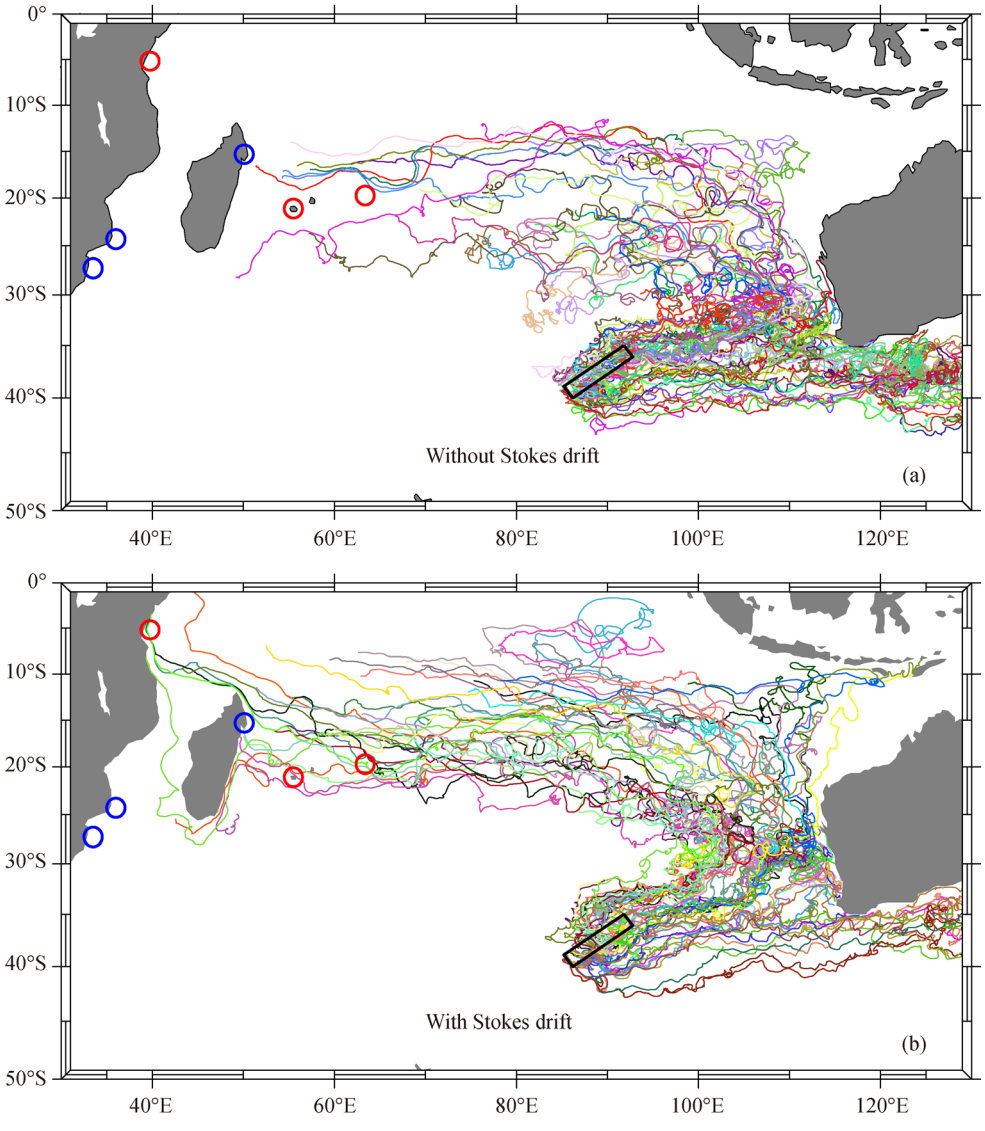

Fig. 5 Trajectories of objects released at the same position with the 61 buoys in Section 4.1.

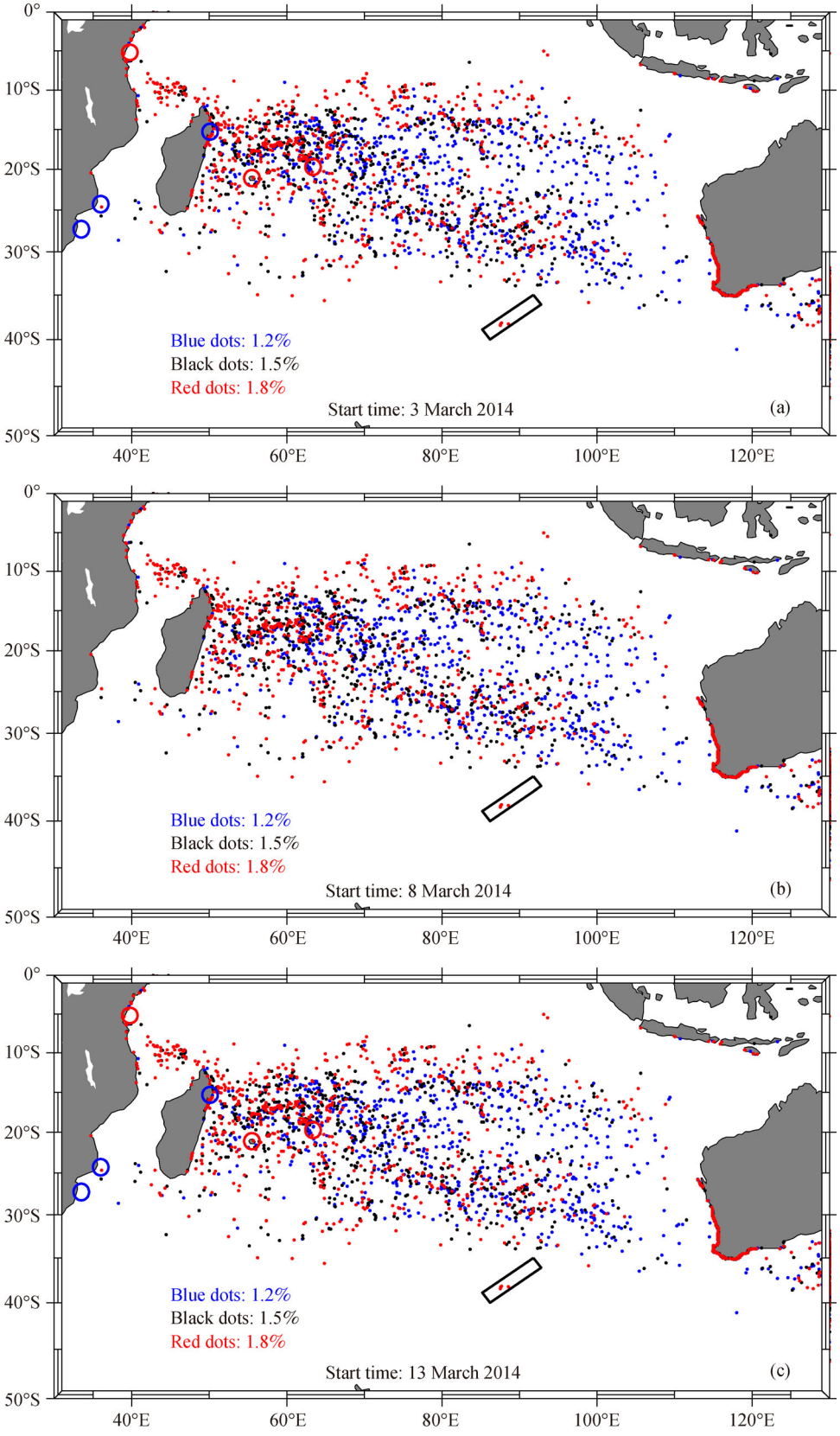

Fig. 6 Simulated location of objects in three cases without Stokes drift. The black box is the possible air crash area; blue, black, and red dots represent objects with leeway factors of 1.2%, 1.5%, and 1.8%, respectively.

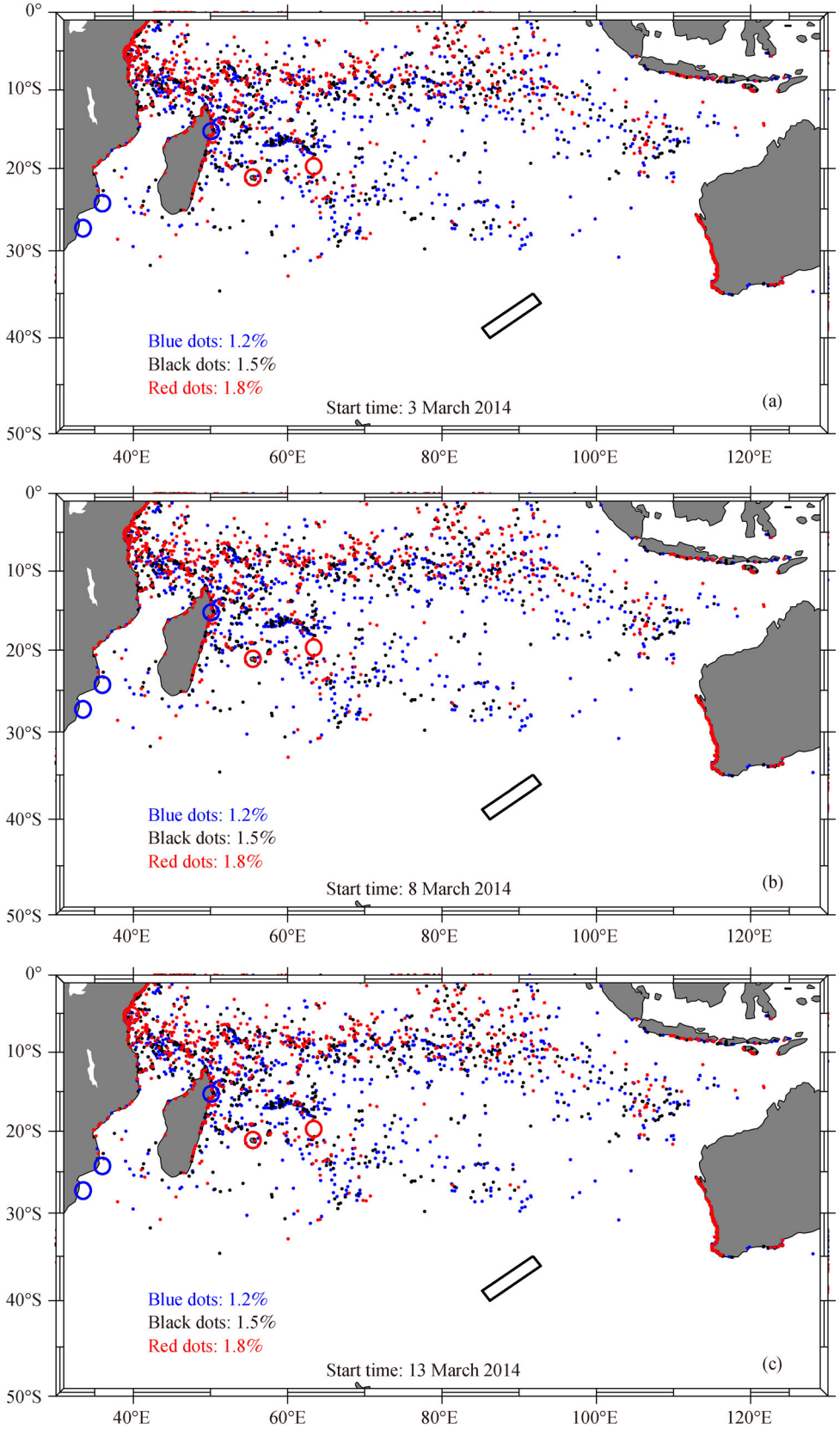

Fig. 7 Simulated location of objects in three cases with Stokes drift. The black box is the possible air crash area; blue, black, and red dots simulate objects with leeway factors of 1.2%, 1.5%, and 1.8%, respectively.

coast of Sumatra. Thus, there is a chance that debris could have drifted from the UWSA along the 7th arc to the areas where pieces of debris were found. The probabilities of 10,044 possible final locations in the areas around Reunion Island, Mauritius, and Tanzania are shown in Table 5, Table 6, and Table 7, respectively. The numbers of objects predicted to reach Reunion Island, Mauritius, and Tanzania are 46, 50, and 192, respectively, and the probabilities that objects end up at these locations are 5‰, 5‰, and 19‰, respectively. As predicted, objects originating in the possible air crash area have higher probabilities of reaching the areas where confirmed or possible pieces of MH370 debris were recovered. Two other reasons for the high probability in Tanzania are that the limitation of the computational domain, and the other is that many objects beach on the coast. The different final destinations for experiments with different leeway factors may be caused by the mainly southeast trade winds in mid–low latitudes.

Table 5 Number and possibility of the objects that finally reached the Reunion Island area (with Stokes drift)

Serial number	Case 1	Case 2	Case 3	Total	Probability
1.2%	7	8	4	19	6‰
1.5%	5	2	8	15	4‰
1.8%	1	6	5	12	4‰
Total	13	16	17	46	5‰
Probability	4‰	5‰	5‰	5‰	

Table 6 Number and possibility of the objects that finally reached the Mauritius area (with Stokes drift)

Serial number	Case 1	Case 2	Case 3	Total	Probability
1.2%	6	10	5	21	6‰
1.5%	5	4	5	14	4‰
1.8%	6	2	7	15	4‰
Total	17	16	17	50	5‰
Probability	5‰	5‰	5‰	5‰	

Table 7 Number and possibility of the objects that finally reached the Pemba Island area (with Stokes drift)

Serial number	Case 1	Case 2	Case 3	Total	Probability
1.2%	18	13	12	43	13‰
1.5%	23	21	16	60	18‰
1.8%	36	29	24	89	27‰
Total	77	63	52	192	19‰
Probability	23‰	19‰	16‰	19‰	

Owing to the long integration time, position differences at each time step accumulate, eventually causing large differences. The results provide a good base reference for assessing debris drifting, although small errors can result in large divergence over time.

To investigate the quantitative influence of Stokes drift and leeway factor, the mean final locations of the objects are shown in Table 8. The difference between the mean final location for results with and without Stokes drift is −17.85°E, 10.54°S, indicating that objects with Stokes drift ended up a mean 2000 km westward and 1200 km northward compared with objects without Stokes drift. In experiments with Stokes drift, the difference in mean final location between leeway factors of 1.2% and 1.5% was −2.1042°E, 0.9660°S, whereas that between 1.5% and 1.8% was −2.17°E, 1.0852°S. In experiments without Stokes drift, there was no significant difference in mean final location among the different leeway factors. It can be seen that the Stokes drift gives the objects a strong positive impetus of drifting to the north and west because it is dominated by the northwestward Stokes drift during the objects' drifting in mid-to-low latitudes.

The UWSA is divided into three parts: south, central, and north. Our model results show that the trajectories of debris originating in the north part are most likely to be consistent with the debris discovered along the east coast of Africa (Fig. 8). The area south of the UWSA (about 40°S) is not suggested as a likely crash site, because most debris from this area is predicted to move east under the

Table 8 Average final locations of all objects with and without Stokes drift

Serial number		With Stokes drift	Without Stokes drift	Difference
Case 1	Exp. 1	72.38°E, −15.06°S	91.95°E, −25.36°S	−19.57°E, 10.30°S
	Exp. 2	70.71°E, −14.03°S	88.45°E, −25.07°S	−17.74°E, 11.04°S
	Exp. 3	69.16°E, −12.68°S	84.92°E, −23.47°S	−15.76°E, 10.79°S
Case 2	Exp. 4	73.04°E, −15.83°S	93.45°E, −25.60°S	−20.41°E, 9.77°S
	Exp. 5	71.95°E, −14.30°S	89.09°E, −24.72°S	−17.14°E, 10.42°S
	Exp. 6	68.93°E, −12.53°S	86.85°E, −24.20°S	−17.92°E, 11.67°S
Case 3	Exp. 7	73.51°E, −16.06°S	92.27°E, −25.55°S	−18.76°E, 9.49°S
	Exp. 8	73.56°E, −14.60°S	90.21°E, −24.95°S	−16.65°E, 10.35°S
	Exp. 9	72.76°E, −13.62°S	89.46°E, −24.66°S	−16.70°E, 11.04°S

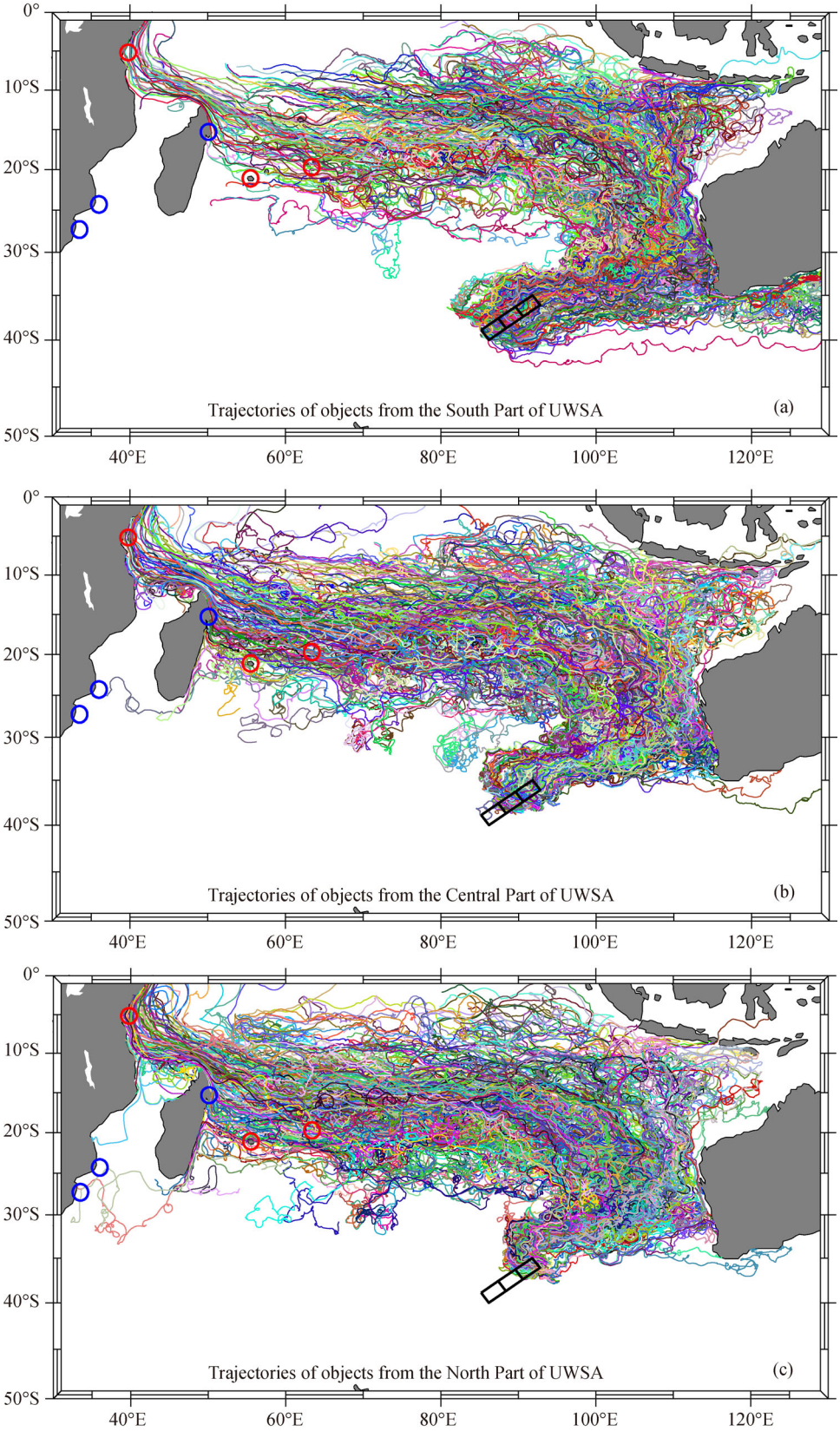

Fig. 8 Trajectories of objects in Experiment 5 (windage, 1.5%; start time, 8 March 2014) from (a) the south part, (b) the central part, and (c) the north part of the underwater search area.

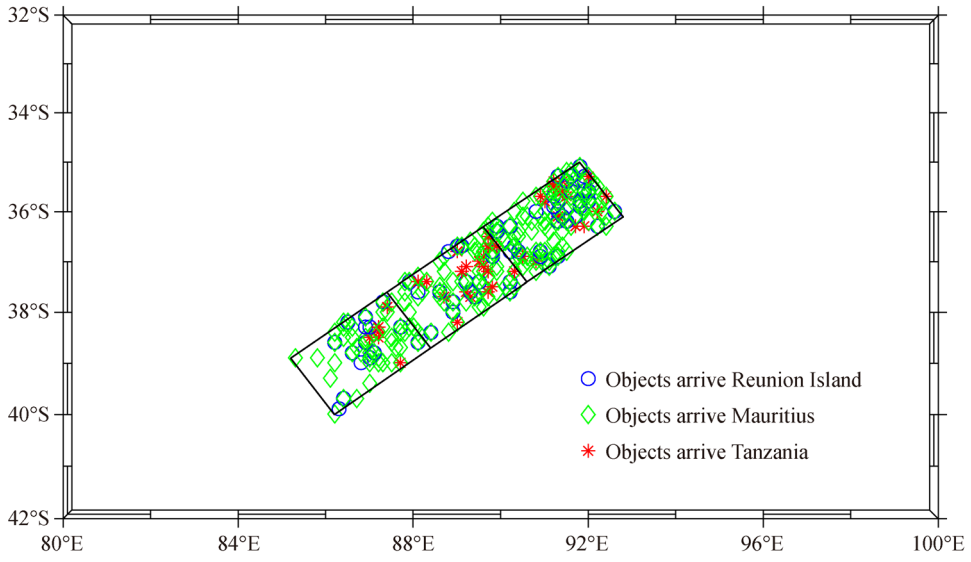

Fig. 9 Initial position of model objects that arrived in the Reunion Island, Mauritius and Tanzania areas in Experiment 5.

control of west wind drift. Similarly, debris from the south part of the UWSA is predicted to move to the east, to the west coast of Australia; however, this area is excluded owing to the many pieces of debris found in Mozambique and South Africa, and the absence of such findings on the west coast of Australia. In conclusion, the north part of UWSA is suggested to be the most likely crash site.

Figure 9 shows the initial positions of the model objects in Experiment 5 that ended up in the Reunion Island, Mauritius, and Tanzania areas. This also shows that the south part of the UWSA is less likely to be the crash site. Highly accurate backtracking should be used to precisely locate the crash site. However, the Indian Ocean is hostile and constantly changing, so no meaningful information can be gathered from the currently available meteorological and oceanic data.

5 Summary and discussion

The results show that debris originating from the UWSA along the 7th arc can drift to the areas in the western Indian Ocean where debris from MH370 had been found. These findings coincide with the actual drifting time of recovered debris, and with data from surface drifters. Numerical simulations that included wind, current, and wave forces support these results. These results indicate that a substantial fraction of assumed debris originating from the UWSA is likely to drift to the north and then turn west. Simulations with and without Stokes drift indicate that the Stokes drift strongly affects the final location of the debris. The results suggest that the north part of the UWSA is the most likely area to be the crash site of MH370.

The study remains unfinished, although the search for MH370 was suspended on 17 January 2017. The biggest challenge in the search for MH370 is the uncertainty of the crash location and time. There is still much work to be done, and also more information needs to be gathered.

Acknowledgements This work is supported by the National Key Research and Development Program of China (No. 2017YFC1404700); the National Natural Science Foundation of China (Grant Nos. 41430963 and 41606005); the Fundamental Research Funds for the Central Universities (No. 201713023). Surface drifter data were provided by the Global Drifter Program. Surface currents data were from Hybrid Coordinate Ocean Model developed by Florida State University (HYCOM). Wave data were provided by the European Centre for Medium-Range Weather Forecasts (ECMWF). Wind data were provided by NOAA's National Centers for Environmental Prediction (NCEP).

References

Allen A A (2005). Leeway divergence, Technical Report CG-D-05-05. US Coast Guard Research and Development Center, Groton, CT, USA

Alves O, Robert C (2005). Tropical Pacific Ocean model error covariances from Monte Carlo simulations. Q J R Meteorol Soc, 131(613): 3643–3658

Ardhuin F, Marie L, Rascle N, Forget P, Roland A (2009). Observation and estimation of Lagrangian, stokes and Eulerian currents induced by wind and waves at the sea surface. J Phys Oceanogr, 39(11): 2820–2838

Ashton C, Shuster Bruce A, Colledge G, Dickinson M (2015). The Search for MH370. J Navig, 68(1): 1–22

ATSB (Australian Transportation Safety Bureau) (2015). MH370 – Definition of Underwater Search Areas. ATSB Transport Safety Report, External Aviation Investigation AE-2014-054, 3 December 2015

ATSB (Australian Transportation Safety Bureau) (2016). MH370 – First Principles Review. ATSB Transport Safety Report, Aviation

External Investigation AE-2014-054, 20 December 2016

Breivik Ø, Allen A A (2008). An operational search and rescue model for the Norwegian Sea and the North Sea. J Mar Syst, 69(1–2): 99–113

Campos R M, Soares C G (2016). Comparison of HIPOCAS and ERA wind and wave reanalysis in the North Atlantic Ocean. Ocean Eng, 112: 320–334

Chassignet E P, Hurlburt H E, Metzger E J, Smedstad O M, Cummings J A, Halliwell G R, Bleck R, Baraille R, Wallcraft A J, Lozano C, Tolman H L, Srinivasan A, Hankin S, Cornillon P, Weisberg R, Barth A, He R, Werner F, Wilkin J (2009). US GODAE: global ocean prediction with the HYbrid Coordinate Ocean Model (HYCOM). Oceanography (Wash DC), 22(2): 64–75

Chaudhuri A H, Ponte R M, Forget G, Heimabach P (2013). A comparison of atmospheric reanalysis surface products over the ocean and implications for uncertainties in air-sea boundary forcing. J Clim, 26(1): 153–170

Cummings J A (2005). Operational multivariate ocean data assimilation. Quarterly Journal of the Royal Meteorological Society, 131(613): 3583–3604

Cummings J A, Smedstad O M (2013). Variational data assimilation for the global ocean, data assimilation for atmospheric. In: Park S K, Xu L, eds. Data Assimilation for Atmospheric, Oceanic and Hydrologic Applications. Springer-Verlag Berlin Heidelberg, 303–343

Dee D P, Uppala S M, Simmons A J, Berrisford P, Poli P, Kobayashi S, Andrae U, Balmaseda M A, Balsamo G, Bauer P, Bechtold P, Beljaars A C M, van de Berg L, Bidlot J, Bormann N, Delsol C, Dragani R, Fuentes M, Geer A J, Haimberger L, Healy S B, Hersbach H, Hólm E V, Isaksen L, Kållberg P, Köhler M, Matricardi M, McNally A P, Monge-Sanz B M, Morcrette J J, Park B K, Peubey C, de Rosnay P, Tavolato C, Thépaut J N, Vitart F (2011). The ERA-Interim reanalysis: configuration and performance of the data assimilation system. Q J R Meteorol Soc, 137(656): 553–597

Eichhorn M, Haertel A (2016). A debris backwards flow simulation system for Malaysia Airlines flight 370. IEEE OCEANS 2016 – Shanghai, 10−13 April 2016

Fox D N, Teague W J, Barron C N, Carnes M R, Lee C M (2002). The modular ocean data assimilation system (MODAS). J Atmos Ocean Technol, 19(2): 240–252

Gao J, Mu L, Wang G S, Li C, Dong J X, Bao X W, Li H, Song J (2016). Drift analysis and prediction of debris from Malaysia Airlines flight MH370. Chin Sci Bull, 61(21): 2409–2418 (in Chinese)

Hui Z, Xu Y (2016). The impact of wave-induced Coriolis-Stokes forcing on satellite-derived ocean surface currents. J Geophys Res Oceans, 121(1): 410–426

Jansen E, Coppini G, Pinardi N (2016). Drift simulation of MH370 debris using supersensemble techniques. Nat Hazards Earth Syst Sci, 16(7): 1623–1628

Joseph S, Wallcraft A J, Jensen T G, Ravichandran M, Shenoi S S C, Nayak S (2012). Weakening of spring Wyrtki jets in the Indian Ocean during 2006–2011. J Geophys Res, 117: C04012

Mo D, Hou Y, Li J, Liu Y (2016). Study on the storm surges induced by cold waves in the northern East China Sea. J Mar Syst, 160: 26–39

Montecinos A, Muñoz R C, Oviedo S, Martínez A, Villagrán V (2017). Climatological Characterization of Puelche Winds down the Western Slope of the Extratropical Andes Mountains Using the NCEP Climate Forecast System Reanalysis. J Appl Meteorol Climatol, 56 (3): 677–696

Philipps O (1977). The Dynamics of the Upper Ocean. Cambridge: Cambridge University Press, 336–337

Polton J A, Lewis D M, Belcher S E (2005). The Role of Wave-Induced Coriolis-Stokes Forcing on the Wind-Driven Mixed Layer. J Phys Oceanogr, 35(6): 444–457

Rahn D A, Garreaud R (2014). A synoptic climatology of the near-surface wind along the west coast of South America. Int J Climatol, 34(3): 780–792

Rimac A, von Storch J S, Eden C, Haak H (2013). The influence of high-resolution wind stress field on the power input to near-inertial motions in the ocean. Geophys Res Lett, 40(18): 4882–4886

Saha S, Moorthi S, Wu X, Wang J, Nadiga S, Tripp P, Behringer D, Hou H T, Chuang H, Iredell M, Ek M, Meng J, Yang R, Mendez M P, van den Dool H, Zhang Q, Wang W, Chen M, Becker E (2014). The NCEP Climate Forecast System Version2. J Clim, 27(6): 2185–2208

Yin Y, Lin X, He R, Hou Y (2017). Impact of mesoscale eddies on Kuroshio intrusion variability northeast of Taiwan. J Geophys Res Oceans, 122(4): 3021–3040

Yu L, Zhong S, Bian X, Heilman W E (2016). Climatology and trend of wind power resources in China and its surrounding regions: a revisit using climate forecast system reanalysis data. Int J Climatol, 36(5): 2173–2188